INL/EXT-12-27937

Fundamental Properties of Salts

Toni Y. Gutknecht
Guy L. Fredrickson

November 2012

The INL is a U.S. Department of Energy National Laboratory
operated by Battelle Energy Alliance

INL/EXT-12-27937
FCRD-PAC-2013-000053

Fundamental Properties of Salts

Toni Y. Gutknecht
Guy L. Fredrickson

November 2012

Idaho National Laboratory
Fuel Cycle Research & Development
Idaho Falls, Idaho 83415

http://www.inl.gov

Prepared for the
U.S. Department of Energy
Office of Nuclear Energy
Under DOE Idaho Operations Office
Contract DE-AC07-05ID14517

SUMMARY

Thermal properties of molten salt systems are of interest to electrorefining operations, pertaining to both the Fuel Cycle Research & Development Program (FCR&D) and Spent Fuel Treatment Mission, currently being pursued by the Department of Energy (DOE). The phase stability of molten salts in an electrorefiner may be adversely impacted by the build-up of fission products in the electrolyte. Potential situations that need to be avoided, during electrorefining operations, include (i) fissile elements build up in the salt that might approach the criticality limits specified for the vessel, (ii) electrolyte freezing at the operating temperature of the electrorefiner due to changes in the liquidus temperature, and (iii) phase separation (non-homogenous solution). The stability (and homogeneity) of the phases can be monitored by studying the thermal characteristics of the molten salts as a function of impurity concentration. Simulated salt compositions consisting of the selected rare earth and alkaline earth chlorides, with a eutectic mixture of LiCl-KCl as the carrier electrolyte, were studied to determine the melting points (thermal characteristics) using a Differential Scanning Calorimeter (DSC). The experimental data were used to model the liquidus temperature. On the basis of the this data, it became possible to predict a spent fuel treatment processing scenario under which electrorefining could no longer be performed as a result of increasing liquidus temperatures of the electrolyte.

CONTENTS

FIGURES

TABLES

ACRONYMS

DOE	Department of Energy
DSC	Differential Scanning Calorimeter
EBR-II	Electron Breeder Reactor-II
ER	Electrorefiner
FCR&D	Fuel Cycle Research & Development
FFTF	Fast Flux Test Facility
FP	Fission Product
Fs	Fissium
HM	Heavy Metal
INL	Idaho National Laboratory
LCC	Liquid Cadmium Cathode
MA	Minor Actinide
Me	Metal
mL	Milliliter
ppm	Parts per million
RCRA	Resource Conservation and Recovery Act
TRU	Transuranic
wt %	Weight percent

FUEL CYCLE RESEARCH & DEVELOPMENT
FUNDAMENTAL PROPERTIES OF SALTS

1. Introduction

The molten salt based pyroprocessing technology is critically important to the United States Fuel Cycle Research and Development (FCR&D) activities (e.g. modified fuel cycle) and non-proliferations. This process was developed for recycling used metallic fuel from the Experimental Breeder Reactor II (EBR-II), which was a sodium-cooled fast reactor using sodium-bonded metallic fuel. In pyroprocessing, the used fuel is anodically dissolved in the molten LiCl-KCl salt, and pure uranium metal is deposited on a steel cathode. Subsequent development of the liquid cadmium cathode (LCC) technology, at the Argonne National Laboratory and the Idaho National Laboratory (INL), allows further recovery of plutonium (Pu), and minor actinides (MA) from the electrolyte. The other two components, namely bond sodium and alkaline earth metals, accumulate in the electrolyte with the progress of the electrorefining run.

Currently, molten 44wt% LiCl-56wt% KCl eutectic salt is being used as the electrolyte, in the electrorefiners (ER) located at INL, to process used nuclear fuel. The ER vessel is 2.25wt%Cr-1wt%Mo steel with an inner diameter and height of approximately 1.0 m and operates at 500°C. This vessel contains a 10-cm-deep pool of molten cadmium, above which lies a 32-cm-deep layer of electrolyte. The electrode assemblies consist of a plain carbon steel cathode mandrel and a stainless steel cruciform anode basket (1).

During electrorefining operations, the liquidus temperature of the electrolyte increases with the accumulation of transuranics (TRUs), fission products (FP), and bond sodium. The extent of the increase in the liquidus temperature can be estimated from the compositions (both predicted and measured) of the salt within the ER as the spent metallic fuel is continuously processed (2). Figure 1 shows how the metal concentrations in the salt increase as a function of the amount of heavy metal fuel processed. The solid lines represent the historic concentrations of the active metals, transuranics, and lanthanides built-up in the electrolyte as a result of processing Experimental Breeder Reactor – II (EBR-II) fuels. The dotted lines represent the projected concentrations as a result of processing Fast Flux Test Facility (FFTF) fuels and EBR-II fuels into the future. The projected electrolyte compositions take into account the decay of plutonium and other elements (3). Figure 1 clearly indicates that both FFTF and EBR-II processing campaigns will exert significant impacts on the thermal properties of the electrolyte.

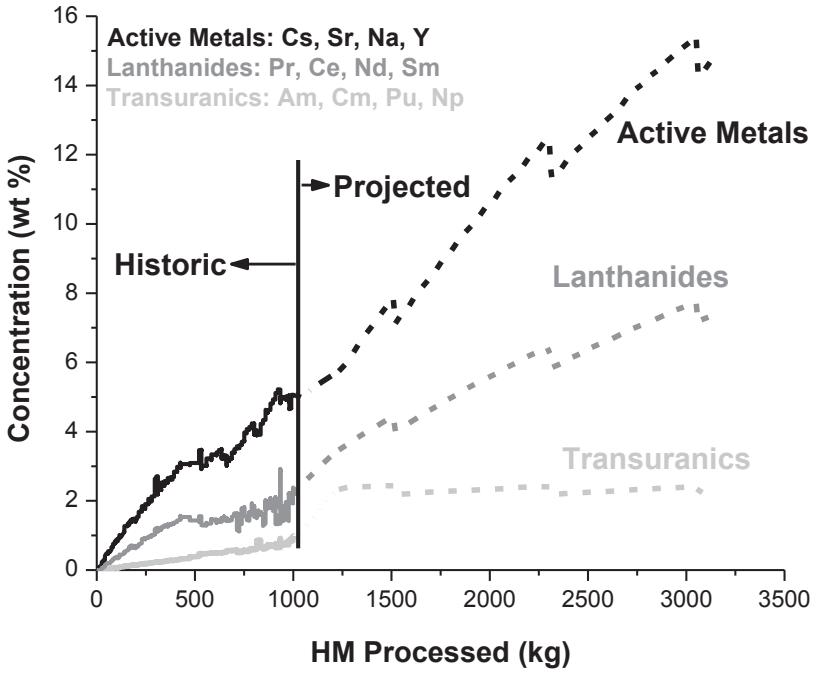

Figure 1: ER salt composition vs. mass of fuel processed.

The projected electrolyte compositions in Figure 1 reflect a campaign of 27 batches of FFTF fuel followed by a significantly larger campaign of 165 batches of EBR-II fuel. A batch refers to an anode basket loading, which is approximately 20 kg of chopped fuel and cladding, while the actinide metal (a.k.a., heavy metal (HM)) content of a batch is approximately 12 kg (4).

The major components of FFTF and EBR-II fuels are listed in Table 1. Uranium, in the form of U-238 (~170 kg) and U-235 (~50 kg), is the major component in the FFTF driver fuel. Zirconium is present because the FFTF fuel is a binary alloy and U-10wt% Zr fuel (5). The composition of EBR-II fuel is U-5wt% Fs, where Fs stands for fissium which is an alloy normally containing 2.4 wt% Mo, 1.9 wt% Ru, 0.3 wt% Rh, 0.2 wt% Pd, 0.1 wt% Zr and 0.01 wt% Nb (5). Total uranium accounts for both U-235 and U-238.

Table 1: FFTF and EBR-II fuel inventories.

	FFTF Fuel Inventory		**EBR-II Fuel Inventory**	
	(g)	**% of total**	**(g)**	**% of total**
Total U	219,588	80.8	1,939,414	94.9
TRU	6,811	2.5	8,605	0.4
Zirconium	31,477	11.6	NA	NA
Sodium	7,061	2.6	52,886	2.6
Other Elements	6,978	2.6	43,214	2.1
Total Fuel Mass	271,915	100.0	2,044,119	100.0

2. Materials and Methods

The liquidus temperature of the electrolyte in the ER is impacted by the impurity buildup of FP, TRU's, and bond sodium. Changes in the liquidus temperature can ultimately affect the useful life of the electrolyte thereby impacting operations and the amount of salt waste generated from the ER. Thermal properties of the electrolyte were analyzed and determined in a Netzsch Model STA 449 F3 Differential Scanning Calorimeter (DSC). Simulated salt samples analyzed in the DSC represented the projected composition of the electrolyte in the ER during processing of FFTF and EBR-II fuels. More than 99 wt% of the ER salt was represented using chlorides of Li, K, Na, Nd, U, Pu, Cs, Ce, La, Pr, Sm, Ba, and Sr. While Gd was used in place of U and Pu, Sr replaced Ba.

Nine samples, each comprised of 15 g, were prepared. These samples were meant to be representative of the bulk composition of the 500 kg inventory of electrolyte in the ER. The chemicals used in the study included ≥ 99.99% anhydrous LiCl-KCl (eutectic composition), $GdCl_3$, NaCl, $NdCl_3$, CsCl, $CeCl_3$, $LaCl_3$, $PrCl_3$, $SmCl_3$, and $SrCl_2$. These metal chlorides represent species present in excess of 0.50 wt% in the ER electrolyte.

Chemicals were stored under argon atmosphere in an MBraun® glove box. The oxygen and moisture concentrations were each maintained below 0.1 parts per million (ppm). All sample preparation steps – measurement, melting and homogenization – were conducted inside the glove box. Calculated quantities of metal chloride salt samples were melted in a 30 mL high-form nickel crucible at 500 to 600°C for approximately one hour. The molten salt sample was cooled and then homogenized using an agate mortar and pestle. Approximately 10 mg of the homogenized sample was place in a gold plated stainless steel DSC crucible. Liquidus and transition temperatures were continuously recorded as the samples were processed under programmed heating and cooling cycles. The experimental parameters for the DSC are listed in Table 2.

Table 2: DSC parameters.

Parameter	Setting
Crucible Material	Au plated Stainless Steel
Crucible Sealing Torque	2.5 N·m
Purge Gas Flow Rate	20 cm^3 min^{-1}
Protective Gas Flow Rate	20 cm^3 min^{-1}
Furnace Atmosphere	UHP Argon
Furnace Material	Platinum Furnace (1500°C max.)
Sample Carrier Material	Platinum/Rhodium
Thermocouple Type	Type S
Calibration	Temperature, Sensitivity
Heating/Cooling Rate	20K min^{-1}, 10 K min^{-1}, 2 K min^{-1}
Sample Size	10 ± 1mg

Out of nine salt samples, two represented electrolyte compositions for processing FFTF fuel and seven represented the electrolyte compositions for processing EBR-II fuel. The composition of each simulated salt sample is given in Table 3. The samples are labeled in reference to the batch of fuel processed. For instance, EBR-II B100 represented the composition of the ER salt after the 100th batch of EBR-II fuel has been processed. Salt compositions are further broken down to their individual metal chloride components in Table 4.

Table 3: Composition of simulated salt samples during fuel processing.

ER Salt Sample	LiCl-KCl, wt%	Actinide Chlorides, wt%	FP Chlorides, wt%	NaCl, wt%
Before FFTF	76.8	9.02	5.84	8.30
After FFTF	70.4	12.0	8.15	9.37
EBR-II B25	66.2	12.5	10.1	11.2
EBR-II B50	59.4	13.6	12.7	14.4
EBR-II B75	54.8	12.3	15.3	17.6
EBR-II B100	53.7	12.2	15.8	18.3
EBR-II B125	48.3	13.3	17.8	20.7
EBR-II B150	44.5	12.1	20.0	23.4
EBR-II B165	44.9	13.1	19.4	22.6

Table 4: Individual salt composition of EBR-II B100 simulated salt sample.

Element	Me in Mk-IV salt, wt%	Calculated MeClx, g	Measured $MeCl_x$, g	Measured Me, g	Measured Me, wt%
Potassium	35.48	4.4089	4.4089	2.3181	35.47
Sodium	16.57	2.7425	2.7432	1.0832	16.58
Uranium (Gd)	12.18	1.3313	1.3313	0.7962	12.18
Lithium	9.20	3.6435	3.6436	0.6013	9.20
Neodymium	6.07	0.6863	0.6865	0.3967	6.07
Plutonium (Gd)	4.55	0.4977	0.4975	0.2975	4.55
Cesium	4.45	0.3667	0.3664	0.2903	4.44
Cerium	3.46	0.3955	0.3956	0.2260	3.46
Barium (Sr)	2.17	0.2564	0.2563	0.1421	2.17
Lanthanum	1.85	0.2126	0.2126	0.1207	1.85
Praseodymium	1.73	0.1979	0.1982	0.1133	1.73
Samarium	1.29	0.1441	0.1446	0.0845	1.29
Strontium	1.00	0.1166	0.1167	0.0651	1.00
Total	100.00	15.0000	15.0014	6.5349	100.00

3. Results

3.1 LiCl-KCl System

Eight salt samples of different compositions from the LiCl-KCl system were prepared and analyzed in the DSC in order to verify the adequacy of the sample preparation technique and performance of the instrument. The measured values were compared against literature values (6-10) for the eutectic and liquids temperatures. Good agreements were obtained between the different sets of data. The eutectic and liquidus temperatures of the samples used for this study are summarized in Table 5.

Table 5: Summary of the LiCl-KCl system data.

Sample	LiCl (mol fraction)	KCl (mol fraction)	Eutectic Temp., °C	Liquidus Temp., °C
1	0.0	1.000	--	769.7
2	.2000	.8000	352.0	682.4
3	.4356	.5644	354.1	522.3
4	.5920	.4080	354.7	354.7
5	.6734	.3266	353.0	426.2
6	.7999	.2001	353.6	511.7
7	.9253	.0747	353.6	578.1
8	1.000	0	--	605.8

Figure 2 shows the experimentally obtained binary phase diagram for LiCl-KCl, constructed with the data from several authors (6-10) and the LiCl-KCl study for this work. A good agreement was obtained between the present data (this work) and the literature data.

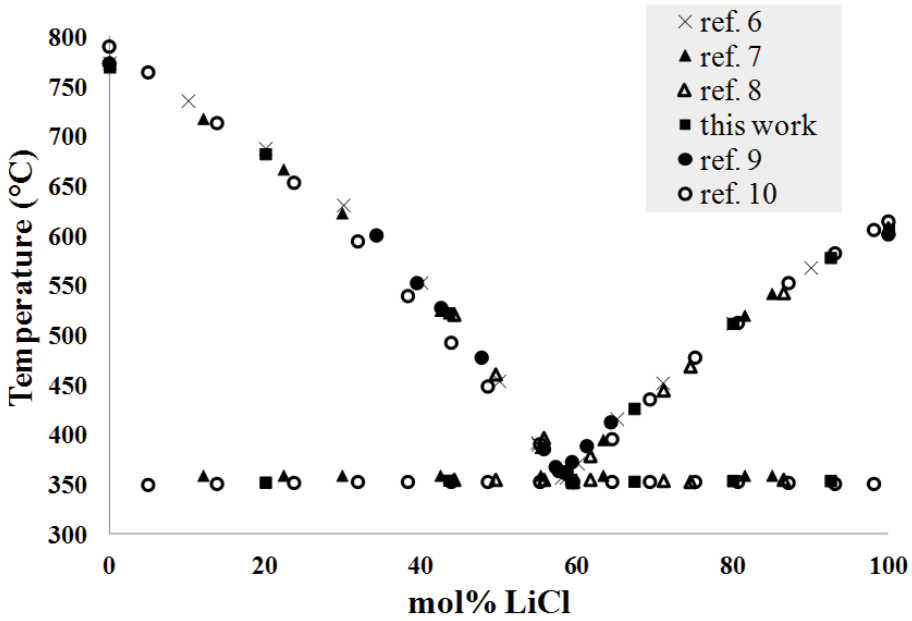

Figure 2: LiCl-KCl phase diagram from various literature sources (6-10) and this work using a heating and cooling rate of 10 K min^{-1}.

3.2 Fuel Processing Study

Figure 3 shows a series of transitions, between the eutectic and liquidus temperatures, for EBR-II B100 sample at a heating rate of 10 K min^{-1} (three heating cycles). A slight variation between the onset and liquidus temperature with different heating rates was observed. It was known that the melting temperature of the ER electrolyte would increase due to a rising impurity concentration from processing used nuclear fuel. However, the extent of the melting temperature increase was not known. DSC analysis of the simulated ER salt samples (FFTF and EBR-II) showed the magnitude of the increase of the melting temperature.

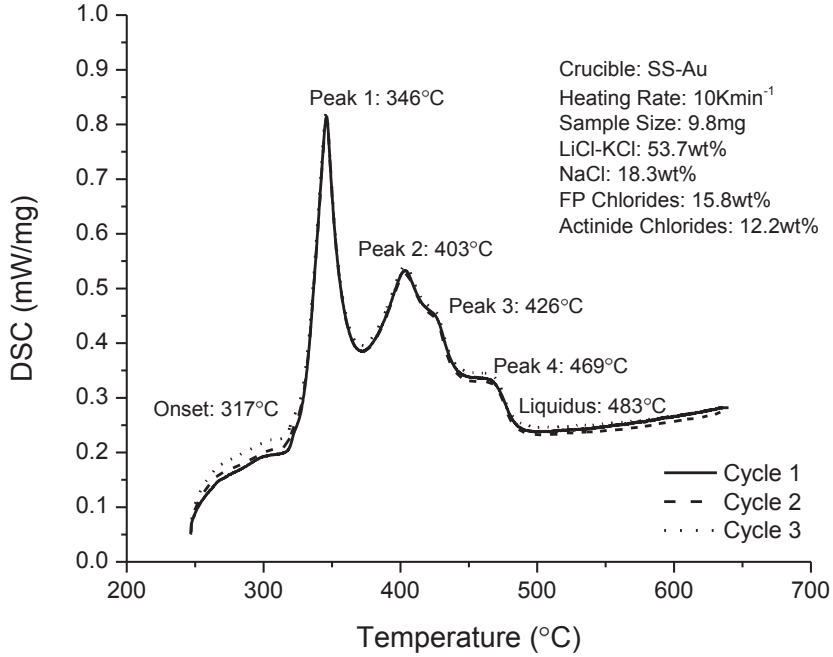

Figure 3: DSC heating curves (heating cycle 1, 2, 3) for the sample EBR-II B100, with a heating rate of 10 K min^{-1}.

The DSC heating curves can be used to determine the average liquidus temperature at different heating rates. Three heating rates (20 K min^{-1}, 10 K min^{-1}, and 2 K min^{-1}) were used for determining the liquidus temperature for the sample EBR-II B100. The x-intercept (Figure 4) is the best interpretation of the liquidus temperature. Thus, 474.9°C was determined to be the heating rate-independent liquidus temperature for sample EBR-II B100.

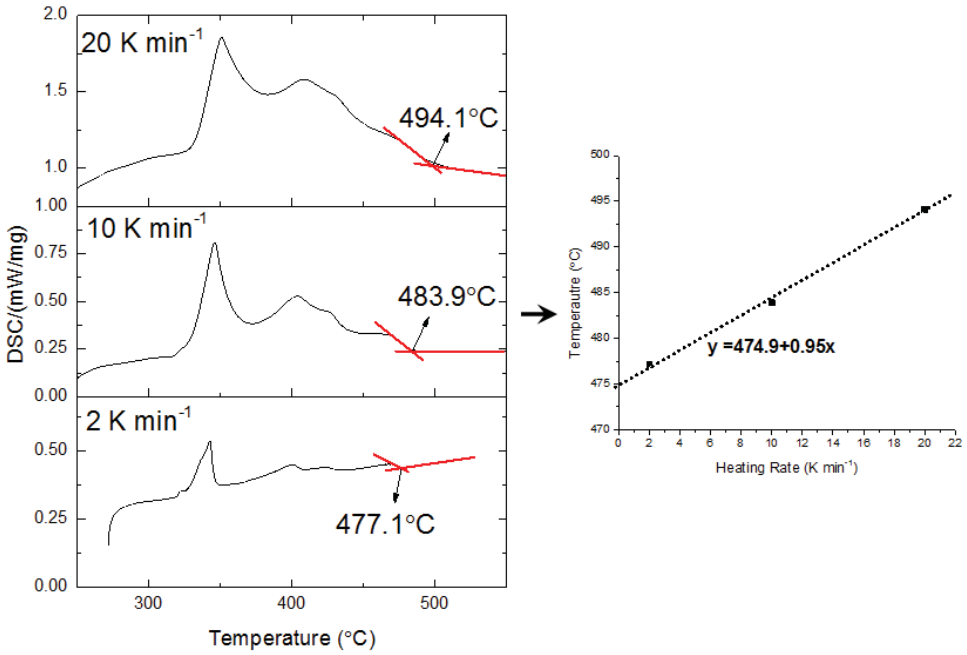

Figure 4: Determination of the liquidus temperature, for the sample EBR-II B100, at multiple heating rates; the melting temperature is determined from the DSC heating curves which are then plotted against the heating rate.

The number and complexity of the peaks, in addition to the eutectic peak, in the DSC thermograms were observed to increase as the impurity load increased. For example, the thermograms of EBR-II B25 and EBR-II B165 contained two and five peaks respectively, suggesting the latter contains a higher number of phases, transitions and/or chemical species. The DSC thermograms, in combination with other complimentary techniques such as powder XRD, SEM-EDX, can be used to determine valuable information on phase transformation, segregation, and immiscibility. However, because of the presence of a number of metal chlorides, the objective of this study was confined to the determination of the eutectic and liquidus temperatures only.

Figure 5 shows the relationship between the liquidus temperature (end of final peak on DSC curve) and impurity concentration present in the electrolyte. The trend in Figure 5 clearly shows that the liquidus temperature increases as used fuel is processed due to increasing impurity concentrations. This was validated using projected electrolyte compositions and surrogates for radioactive and Resource Conservation and Recovery Act (RCRA) metals, i.e. Barium. Actual liquidus temperatures of the electrolyte during the processing of FFTF and EBR-II used fuel may vary.

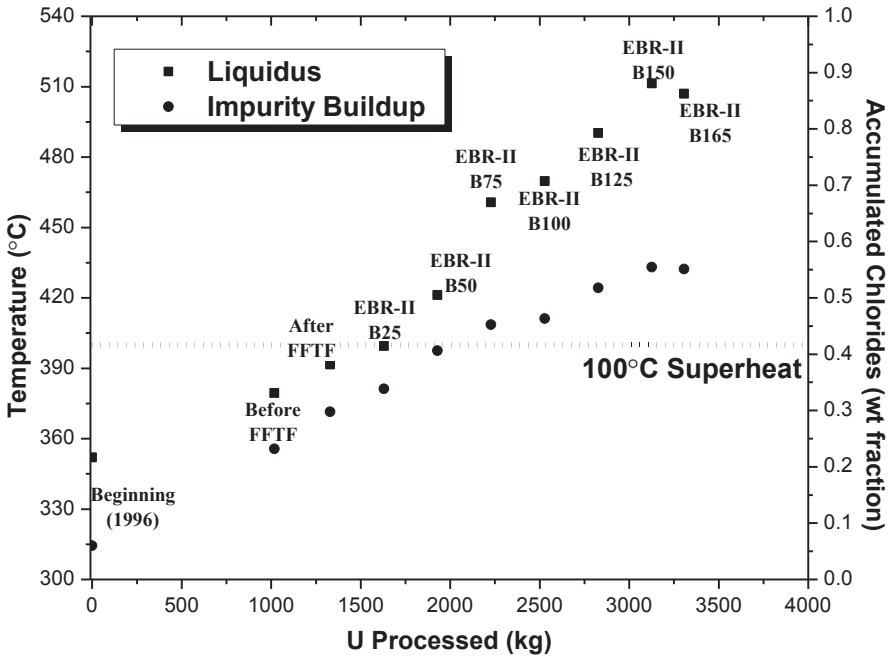

Figure 5: Liquidus temperature as a function of impurity concentration in simulated salt samples.

The ER operates at 500°C for current electrorefining operations. To ensure safe operating conditions, it may be recommended that, for example, the electrorefiner not be operated with less than 100°C superheat. Superheat is defined as the difference between the ER operating temperature and the liquidus temperature of the electrolyte. Figure 5 suggests that the ER electrolyte will have less than 100°C of superheat after the processing of EBR-II B25. One possible solution to lower the liquidus temperature of the ER salt is to remove some portion of the impurity laden salt and replace it with fresh LiCl-KCl eutectic salt. And, it may be worthwhile to remove the bond sodium from the fuel, prior to electrorefining operations, as sodium is one of the major contributors to the increase in the liquidus temperature.

4. Discussion

It may be possible to predict the melting temperature of the salt samples, investigated in the present study, using a model, originally developed by Sangster and Pelton for the ternary system LiCl-KCl-NaCl if an assumption is made that the concentrations of all salts other than LiCl and KCl are represented by NaCl (11). This means, NaCl can represent the combination of $SrCl_2$, CsCl, $BaCl_2$, $LaCl_3$, $CeCl_3$, $PrCl_3$, $NdCl_3$, $SmCl_3$, $GdCl_3$, and of course NaCl. As per the model, developed by Sangster and Pelton (11, 12), the nearest neighbor interactions are assumed to be approximately the same distance apart, which is the case for monvalent ions such as Li, K, and Na. In the present study, the salt samples were a combination of mono, di and tri valent species. Nonetheless it may still be possible to use the model assuming the nearest neighbor interaction parameters for multivalent species is dominated (accounted for) by the NaCl nearest neighbor interaction parameters.

Modeled liquidus temperatures, listed in Table 7, were extracted from the ternary liquidus projection, developed by Sangster and Pelton (11). The ratio of LiCl-KCl remained constant (44 wt% LiCl) as the NaCl concentration increased. The NaCl concentration in the ternary LiCl-KCl-NaCl was assumed to be

equal to the sum of all species in solution except LiCl and KCl (representative NaCl in Table 7). For example 0.1 mol of $NdCl_3$ would be represented as 0.1 mol NaCl. Values for the modeled liquidus temperature along with the experimental liquidus temperature, representative NaCl concentration and other metals chloride concentrations are listed in Table 7. The experimental liquidus temperature was taken from the DSC curves of simulated ER salt samples. The representative NaCl concentration is the other metal chloride concentration plus the experimentally added NaCl concentration.

Table 7: Composition and liquidus temperature of modeled and simulated salt samples.

Sample	Representative NaCl (mol fraction)	Other Metal Chloride (mol fraction)	Modeled Liquidus Temperature (°C)	Experimental Liquidus Temperature (°C)
Before FFTF	0.128	0.038	400	376
After FFTF	0.161	0.055	425	392
EBR-II B25	0.194	0.067	450	406
EBR-II B50	0.250	0.077	495	433
EBR-II B75	0.299	0.084	520	470
EBR-II B100	0.310	0.086	525	475
EBR-II B125	0.361	0.099	555	499
EBR-II B150	0.404	0.105	575	516
EBR-II B165	0.397	0.106	575	513

Figure 6, is a plot of the liquidus temperature versus the NaCl concentration. The liquidus temperature is based on the representative composition of NaCl present in the LiCl-KCl-NaCl system. Figure 6 shows the difference (in temperature) between the modeled and experimentally obtained liquidus temperatures. A linear fit was applied to both sets of data, yielding the following two equations:

where x is the representative mol fraction of NaCl and its values are given in Table 7 for all simulated salt samples.

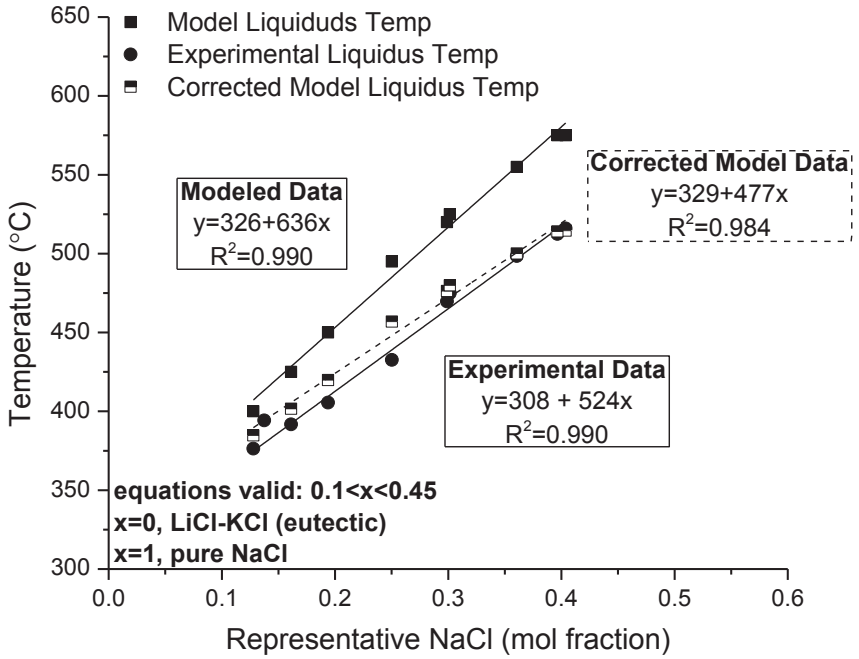

Figure 6: Quasi-Binary phase diagram representing NaCl and LiCl-KCl eutectic. Composition vs. liquidus temperatures for modeled, experimental and corrected modeled systems.

The modeled data is based on the simple ternary system, LiCl-KCl-NaCl, which has been studied by others (11). Experimental data is based on a complex system, composed of KCl, LiCl, NaCl, $SrCl_2$, CsCl, $BaCl_2$, $LaCl_3$, $CeCl_3$, $PrCl_3$, $NdCl_3$, $SmCl_3$, and $GdCl_3$. Upon introduction of a correction factor to the modeled data, it may become possible to account for the interactions from salt constituents other than monovalent KCl, LiCl, and NaCl. The correction factor (β) is applied to the model data to account for the actual NaCl concentration in the salt and can be expressed as:

or (equivalently)

Introduction of the correction factor to the model data reduces the error due to the overestimation or oversimplification of the liquidus temperature by way of reducing the concentration of NaCl (representative NaCl concentration), accounted for in the modeled data to the actual concentration (experimentally added = Representative NaCl Conc. – Other Metal Chloride Conc.) of NaCl that comprised the simulated ER salt samples. The corrected data are represented by half filled black squares in Figure 6 and can be described by the following linear equation:

A simple check of equation 5 shows that the assumptions made for the corrected model have been proven for values $0.1 < x < 0.45$ (where x is the representative NaCl mol fraction). At $x = 1$, the composition of the quasi binary system shown in Figure 6 would be 1.0 mol fraction (pure) NaCl having a melting temperature of 801°C. When $x = 1$ in Equation 5, the liquidus temperature predicted by the corrected

model is 806°C. Thus, the corrected modeled value is off by approximately 5°C. For x = 0 (pure) LiCl-KCl the melting temperature should be approximately 353°C. Using equation 5 when x = 0 the melting temperature of LiCl-KCl is predicted by the corrected model to be 329°C. Clearly there are limitations to the model at low concentrations of NaCl.

As the concentration of NaCl increases in the corrected model the accuracy of the predicted liquidus temperature also increases. Table 8 shows the corrected modeled liquidus temperature, experimental liquidus temperature, and the difference between them. The modeled value is off by at most 25°C and as little as 1.5°C for compositions of representative NaCl in the ER simulated salt samples between 0.10 and 0.45 mol fraction. Modeled, experimental and corrected model data can be fitted using linear functions all giving $R^2 > 0.98$.

Table 8: Correction factor (β) and values for the corrected model liquidus temperature compared to the experimental liquidus temperature.

Sample	β (°C)	Corrected Model Liquidus Temperature (°C)	Experimental Liquidus Temperature (°C)	Experimental – Corrected Model (°C)
Before FFTF	15.2	384	376	8.40
After FFTF	23.4	402	392	9.93
EBR-II B25	30.2	420	406	14.4
EBR-II B50	38.1	457	433	24.3
EBR-II B75	43.7	476	470	6.62
EBR-II B100	45.2	480	475	4.95
EBR-II B125	54.9	500	499	1.56
EBR-II B150	60.4	515	516	-1.38
EBR-II B165	61.0	514	513	1.55

β is expected to account for the change in liquidus temperature due to the formation of complex species, consisting of a mixture of Sr, Cs, Ba, La, Ce, Pr, Nd, Sm, and Gd for which information does not readily exist in open literature. Modifying the model data to predict the liquidus temperature of the complex simulated ER salt using a simple monvalent ternary LiCl-KCl-NaCl system has proven that it is possible to predict thermal properties of complex, unknown systems containing multivalent species with the help of a modified version of a model that is being used for simple ternary systems.

The present study has provided a strong platform for similar research and is a good foundation for experiments to aid in predicting the thermal behavior of a system using actual radiological components. A logical extension of this study would therefore be to repeat the same set of experiments using UCl_3 and $PuCl_3$. A similar experimental setup can be used to generate thermodynamic data on systems of interest to pyroprocessing including but not limited to: LiCl-KCl-UCl_3, LiCl-KCl-$PuCl_3$, LiCl-KCl-$NpCl_3$, etc.

5. Conclusions

The liquidus temperature of the ER electrolyte increases as the wt% of impurities (actinide, FP, and bond sodium) increase. Although this general trend was expected, the exact nature of the trend, as a function of type and mass of spent fuel processed in the ER, was previously unknown. This study was the first of its kind to investigate the effects of electrorefining operations on the thermal characteristics the of ER electrolyte. From the present study, it can be concluded that in order to maintain a 100°C of superheat temperature the impurity chloride concentration in the ER electrolyte should not be greater than 35 wt% For metal fuels (FFTF and EBR-II) scheduled to be processed through the Mk-IV ER at the INL the ER electrolyte will contain greater than 35 wt% of metal chloride impurities after processing all FFTF fuel and up to the 25th batch of EBR-II fuel. At that time it may be necessary to remove and/or replace some of the electrolyte in order to reduce the impurity concentration built up and restore back the required degree of superheat temperature. The present work also suggests that the electrolyte in the ER is a function of NaCl concentration. Therefore to prolong the life of the eutectic electrolyte, it may prove to be beneficial to remove the bond sodium from the spent fuel prior to the electrorefining of the used metallic fuel.

6. Acknowledgements

Financial assistance provided by the U.S. Department of Energy (US-DOE), Idaho National Laboratory (INL), Fuel Cycle Research and Development Program (FCR&D) and the Republic of Korea (ROK), Korean Atomic Energy Research Institute (KAERI), Ministry of Education, Science and Technology (MEST) through the work package # FT-12IN110509, “Critical Gap R&D – INL: Fundamental Properties of TRU – Bearing Salt” are gratefully acknowledged. The authors would also like to thank all those persons, both at the Idaho National Laboratory, the University of Idaho, and Netzsch who provided assistance to this work.

7. Literature Cited

1. Li, S. X., Johnson, T. A., Westphal, B. R., Goff, K. M., and Benedict, R. W. (2005). Electrorefining Experience for Pyrochemical Processing of Spent EBR-II Driver Fuel. *Global,* Tsukuba, Japan.
2. Yoo, T. (2011a). Updated Modeling and Simulation of FFTF Treatment Strategies. *Unpublished manuscript.*
3. Yoo, T. (2011b). Updated Modeling and Simulation of Fissium Treatment Strategies. *Unpublished manuscript.*
4. Westphal, B. R., Vaden, D., Li, S. X., Fredrickson, G. L., and Mariani, R. D. (2009). Fate of Noble Metal Fission Products during Electrorefining. *Proceedings of Global,* Paris, France. (9309)
5. Burkes, D. E., Fielding, R. S., Porter, D. L., Crawford, D. C., and Meyer, M. K. (2009). A US Perspective on Fast Reactor Fuel Fabrication Technology and Experience Part I: Metal fuels and assembly design. *Journal of Nuclear Materials*, 389(3), p458.
6. Basin, A.S., Kaplun, A.B., Meshalkin, A.B. and Uvarov, N.F. (2008). The LiCl-KCl Binary System. *Russian Journal of Inorganinc Chemistry*. 53(9) p1509
7. Keitel, H. Über die ternären Systeme aus Lithium-, Kalium-, Rubidiumchlorid und Kalium-, Rubidium, Cäsiumchlorid. Neues Jahrb. Mineral., Geol., Beilage-Bd. A, 52, 378–423 (1925).
8. Richards, T.W. and Meldrum, R.W. (1917). The Melting Point of the Lithium, Rubidium, and Caesium, and the Freezing Points of Binary and Ternary Mixtures of These Salts, Including also Potassium and Sodium Chloride. *Journal of the American Chemical Society*. 39 (9), p1816
9. Elchagardus, E. and Laffite, P. (1932) Etude thermique des systems ClK-Cl_2Ba et ClK-ClLi. *Bulletin de la Societe Chimique*. 51, t. 156p1572
10. Zemczuzny, E., and Rambach, F., (1910). Schmelzen der Alkalichloride. *Zeitschrift für anorganische Chemie*. 65(1)p403
11. Sangster J. and Pelton, D. (1991) Thermodynamic Calculation of Phase Diagrams of the 60 Common-Ion Ternary Systems Containing Cations Li, Na, K, Rb, Cs and Anions F, Cl, Br, I. *Journal of Phase Equilibria,* 12(15), p511
12. Sangster J. and Pelton, D. (1987). Phase Diagrams and Thermodynamic Properties of the 70 Binary Alkali Halide Systems Having Common Ions. *Journal of Physical and Chemical Reference Data*. *16*, p509.

Appendix A:

Masters Thesis